



# Design of compact tri and quad band band-pass filters using stub loaded resonators for wireless applications

Abdul Sami<sup>1</sup> · MuhibUr Rahman<sup>2</sup> · Shahid Bashir<sup>3</sup>

© Springer Nature Switzerland AG 2019

## Abstract

A compact tri and quad band band-pass filters (BPFs) utilizing stub loaded resonators is presented for wireless applications. The proposed resonator has been designed and analyzed using even–odd mode analysis due to its symmetrical geometry. Open-ended stubs are loaded at an appropriate position in the dual-mode resonator to achieve tri and quad passbands. To reduce the circuit size and create transmission zeros at our desired frequencies, a symmetrical meandered shape resonator is loaded with open-ended identical stubs which are bent towards each other. The proposed BPFs are tune to operate at GSM (900 MHz), LTE (2300 MHz), WiMAX (3.5 GHz), and WLAN (5.4 GHz) bands. Significant improvements are observed in terms of circuit size, 3-dB fractional bandwidth, insertion loss, and transmission zeros. To check the validity of the proposed tri and quad BPFs, these are simulated, fabricated and measured. The simulated and measured results are compared and strong agreement is observed. The proposed filters can be prospective candidates for wireless communication applications.

**Keywords** Stub loaded resonators (SLR) · Band-pass filters (BPFs) · Triple BPF · Quad BPF · Even and odd mode analysis · WLAN (wireless local area network) · WiMAX (worldwide interoperability for microwave acces) · LTE (long term evolution)

## 1 Introduction

After the commercialization of 3G and 4G, the demand for multiband wireless transceivers is becoming more and more desirable. Multiband transceivers are extremely essential for smartphone applications because of their low cost and small size. Filters are having a vital part in the RF front end to obtain the preferred and high-quality signals. In order to provide smooth communication by a multiband transceiver, it is necessary to have BPFs which have small circuit size and high selectivity to avoid any interference with nearby frequency bands. In this regard, a lot of research has been performed and different techniques and methodologies have been adopted to realize multi-band BPFs. Extensive research work has been done

on dual BPF using techniques such as coupling matrix, loaded stub and frequency transformation. But most of these BPF design techniques were applicable to specific pass-band responses [1–3]. A multiband BPF was designed and then integrated with Ultra-Wideband (UWB) antenna to achieve band-notch functionality [4]. It shows that multiband bandpass filters have many direct and indirect advantages and can be used in different applications for various purposes.

Similarly, in [5, 6] dual band-pass filters are developed using DGS (Defected Ground structures) and Stepped Impedance Resonators (SIRs) coupling techniques. But the reported works have a narrow bandwidth, large circuit size and high insertion loss for both passbands. Recently, a dual notched band filter response is reported

✉ MuhibUr Rahman, muhibur.rahman@polymtl.ca | <sup>1</sup>Department of Electrical Engineering, College of Electrical and Mechanical Engineering, NUST, Islamabad, Pakistan. <sup>2</sup>Department of Electrical Engineering, Ecole Polytechnique de Montréal, University of Montreal, Montreal, QC H3T 1J4, Canada. <sup>3</sup>Department of Electrical Engineering, University of Engineering and Technology, Peshawar, Pakistan.



for UWB application with the help of four open stubs which are attached with the microstrip patches in [7]. In [8], a tri-band band-pass filter has been designed using open stubs and DGS. The presented filter has poor selectivity and large circuit size due to lack of transmission zeros. A ring resonator having three degenerate modes is employed to achieve a tri-band response in [9]. However, this technique has limited independent control of passbands. This limitation has been removed by implementing SLR in the bandpass filter [10].

A tri-band BPF is also developed in [11], by employing SIR with loaded stubs. However, it has narrow bandwidth and contains only two transmission zeros which decrease the sharp selectivity of the filter. Recently, a tri-band response is achieved by means of a combination of SLR termed as SLDMRs [12]. Two SLDMRs combined with intra-resonator coupling between inner and outer rings are utilized to obtain a triple passband response. However, the size of the filter is large and five transmission zeros are achieved. Multi-mode stub loaded quarter wave resonators were utilized to realize tri-band filters for wireless applications [13]. The author in [14] offers a very compact wide band bandpass filter using quasi-elliptic resonator in combination with DGS. The presented filter is advantageous in terms of insertion loss, 3-dB fractional bandwidth, and with two transmission zeros. The proposed filter was implemented in frequency scanning beam array antenna to increase its bandwidth. Also, in [15] a triple band BPF to operate at GSM-900, GSM-1800, and GPS (1.575 GHz) was presented. However, it has a serious issue of losses in one of the passband due to the matching of loaded and unloaded quality factor. Also, a microstrip low-pass filter is designed in [16] with a very wide stopband. This filter is advantageous and can be transformed to corresponding passbands by utilizing SRR and ring resonator with circular geometry.

Limited research has been reported on quad-band BPFs. In [17], a technique of multiband BPF was developed by first designing a UWB bandpass filter and then transforming into different bandpass filters. Single, dual, triple, and quad-band BPF is designed using the developed technique and also placement of transmission zeros is analyzed. All the passbands can be controlled parametrically and a selective passband response can be achieved. This technique is very simple, however, it needs a large circuit area for designing higher order filters. Also, in [18] four passbands are achieved using the technique of splitting a single wideband into multiple passbands. This technique is complex and independent tuning of each passband is challenging. The use of SIR in multiband BPF is also utilized and different geometries are developed in [19–21]. They utilized higher

order modes to create additional pass-bands. Also, such an approach generates an additional loss and greatly increases the overall size of the circuit.

In this manuscript, first a tri-band BPF response is achieved using dual-mode meandered shape symmetrical resonator loaded with open-ended stubs. They are further bent towards each other to reduce overall circuit area and to enhance the selectivity of the pass-bands with the help of introducing transmission zeros in the stop-bands. As the design is symmetric, so even and odd mode analysis is being implemented and the corresponding resonance frequencies are achieved. The pass-bands of the BPFs can be easily tuned and shifted. The quad-band BPF response is made possible by incorporating two more identical open-ended stubs in the existing tri-band BPF design. The proposed BPFs are tuned to GSM-900, LTE-2300, WiMAX (3.50 GHz) and WLAN (5.40 GHz) wireless applications. Considerable improvements are observed in the case of overall circuit size, 3-dB fractional bandwidth, insertion loss, and high skirt selectivity. The proposed designs are simulated, fabricated and measured and the corresponding frequency response in each case is provided.

## 2 Resonator analysis

A basic SLR comprising of one shorted stub and six open stubs is provided in Fig. 1. It is further decomposed into even and odd mode circuits as shown in Fig. 1b, c, respectively. This even and odd mode can further be decomposed into eight resonant circuits as shown from Fig. 1d–k, respectively. Now, the resonant odd and even mode frequencies are calculated using the following equations:

$$f_{even1} = \frac{(2n-1)c}{4(L_1 + L_2 + L_3 + L_4 + L_5)\sqrt{\epsilon_{eff}}} \quad (1)$$

$$f_{odd1} = \frac{(2n-1)c}{4(L_1 + L_2 + L_3 + L_4)\sqrt{\epsilon_{eff}}} \quad (2)$$

$$f_{even2} = \frac{(2n-1)c}{4(L_2 + L_3 + L_4 + L_5 + L_6)\sqrt{\epsilon_{eff}}} \quad (3)$$

$$f_{odd2} = \frac{(2n-1)c}{4(L_2 + L_3 + L_4 + L_5)\sqrt{\epsilon_{eff}}} \quad (4)$$

$$f_{even3} = \frac{(2n-1)c}{4(L_3 + L_4 + L_6 + L_5)\sqrt{\epsilon_{eff}}} \quad (5)$$

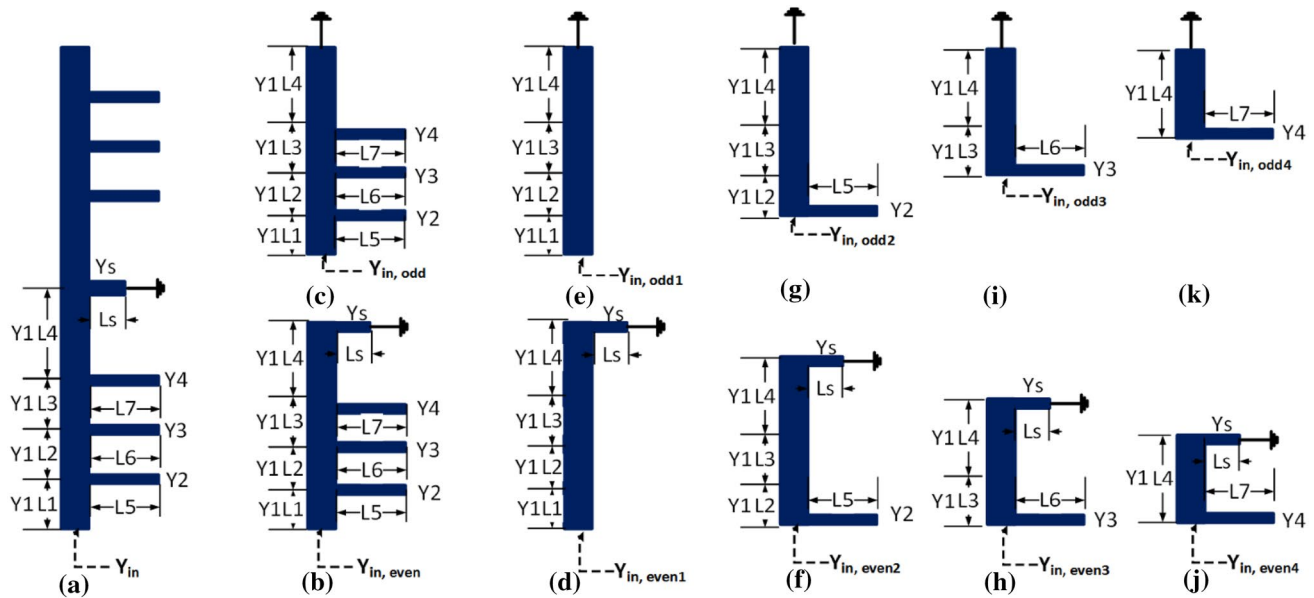


**Fig. 1** Proposed SLR decomposition into corresponding even and odd mode equivalent developed circuits, **a** Configuration of the proposed SLR, **b** Even-mode eqvt. Circuit, **c** Odd-mode eqvt. Circuit, **d–k** Decomposition of **(b)** and **(c)**

$$f_{odd3} = \frac{(2n - 1)c}{4(L_3 + L_4 + L_6)\sqrt{\epsilon_{eff}}}$$

$$f_{even4} = \frac{(2n - 1)c}{4(L_4 + L_7 + L_s)\sqrt{\epsilon_{eff}}}$$

$$f_{odd4} = \frac{(2n - 1)c}{4(L_4 + L_7)\sqrt{\epsilon_{eff}}}$$

where, 1, 2, 3, 4 in the subscript represents the corresponding bands,  $L_s$  and  $L_1-L_7$  signifies the lengths of the corresponding line with respective characteristic admittances of  $Y_s$  and  $Y_1-Y_7$ . Moreover,  $c$  represents speed of light,  $n = 1, 2, 3, \dots$ , and  $\epsilon_{eff}$  shows the effective permittivity of the substrate. It must be noted that proposed technique can be extended easily to  $N$ -passbands as well.

### 3 Approach for designing tri-band BPF

Based on the above analysis performed in Eqs (1)–(8), a compact tri-band BPF is developed as shown in Fig. 2. Four open stubs are loaded in a symmetrical manner and one short ended stub is loaded at the middle of the proposed dual mode resonator. The short ended stub at the middle of the circuit is shorted with the ground plane utilizing via hole. The symmetrical meandered resonator is loaded with open stubs

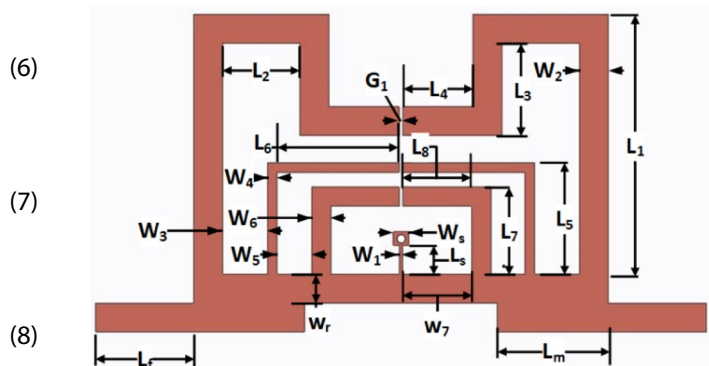


**Fig. 2** Proposed tri-band BPF configuration

which are extended towards each other in order to reduce the filter size and make transmission zeros in the stop-band region to get sharp selectivity. The transmission zeros are created in the frequency band when the input impedance of the identical open stubs equal to zero [17] which will act as the virtual ground at the input points. The input signal is shorted and cannot transmit to the output port. The position of the transmission zeros in frequency band created by the resonator and the loaded identical open stubs is given by the following equation:

$$\cot \theta_s = 0 \tag{9}$$

Equation (9) can also be transformed into the following form:

$$f_{zt} = \frac{n\pi f_0}{2\theta_s} \tag{10}$$

where  $n = 1, 3, 5$ ,  $f_{zt}$  is the frequency of the transmission zero,  $\theta_s$  signifies the electrical length of the identical open stubs and resonator and  $f_0$  is the design frequency. So the length of the resonator and loaded open stubs are controlling the center frequencies of all the pass-bands and also the position of the transmission zeros in the stop-bands.

In order to validate this,  $L_1$  is varied from 13.1 to 16.1 mm and  $L_3$  from 3.6 to 6.6 mm at the same time. The simulated results are plotted in Fig. 3a, which shows that decreasing the lengths  $L_1$  and  $L_3$  will shift the center frequency and position of transmission zeros,  $T_{z1}$ , and  $T_{z2}$  to high frequency. These parameters can tune the first band to the desired frequency band. Also, changing the position of transmission zeros  $T_{z1}$  and  $T_{z2}$  due to the change in length of resonator also affect the lower frequency of the second passband as well. Thus the lower frequency of the second pass-band can also be adjusted by proper positioning of transmission zeros  $T_{z1}$  and  $T_{z2}$ . In Fig. 3b, length  $L_6$  of the loaded open stubs is changed from 6.575 to 8.075 mm. The simulated results for different values of  $L_6$  show that center frequency of band 2 shifts from a lower frequency to high frequency and also change the position of transmission zeros  $T_{z3}$  and  $T_{z4}$  from lower to a higher frequency when the length of  $L_6$  is decreased from 8.075 to 6.575 mm. The changing position of transmission zeros  $T_{z3}$  and  $T_{z4}$  also shift the lower frequency of third pass-band. The third passband lower frequency can be tuned with the help of transmission zeros  $T_{z3}$  and  $T_{z4}$ . In the same way, length  $L_8$  of the loaded open stubs is varied from 2.75 to 4 mm as shown in Fig. 3c. Decreasing  $L_8$  from 4 to 2.75 mm tune the center frequency from lower to higher frequency and also shift the position of the transmission zeros  $T_{z5}$  and  $T_{z6}$  to high frequency in the stop-band region. Therefore, it is evident from the simulations, that all the three passbands of the tri-band BPF can be properly tuned to preferred frequency bands by the length of the resonator and loaded open stubs.

Also, the spacing between the identical stubs denoted by  $G_1, G_2$ , and  $G_3$ , allow capacitive coupling between the stubs. The capacitance between the stubs increases as the spacing between the stubs decreases according to [17]. So tri-band BPF is simulated for different values of  $G_1$  and  $G_2$  as shown in Fig. 4a, b). It is evident from Fig. 4a that when the value of  $G_1$  increases, the transmission zeros  $T_{z1}$  and  $T_{z2}$  come closer in the  $S_{21}$  plot of the frequency response. Same is the case for  $G_2$  where transmission zeros  $T_{z3}$  and  $T_{z4}$  come close to each other when the value of  $G_2$  increases. Hence, when the capacitance between the identical stubs decreases the transmission

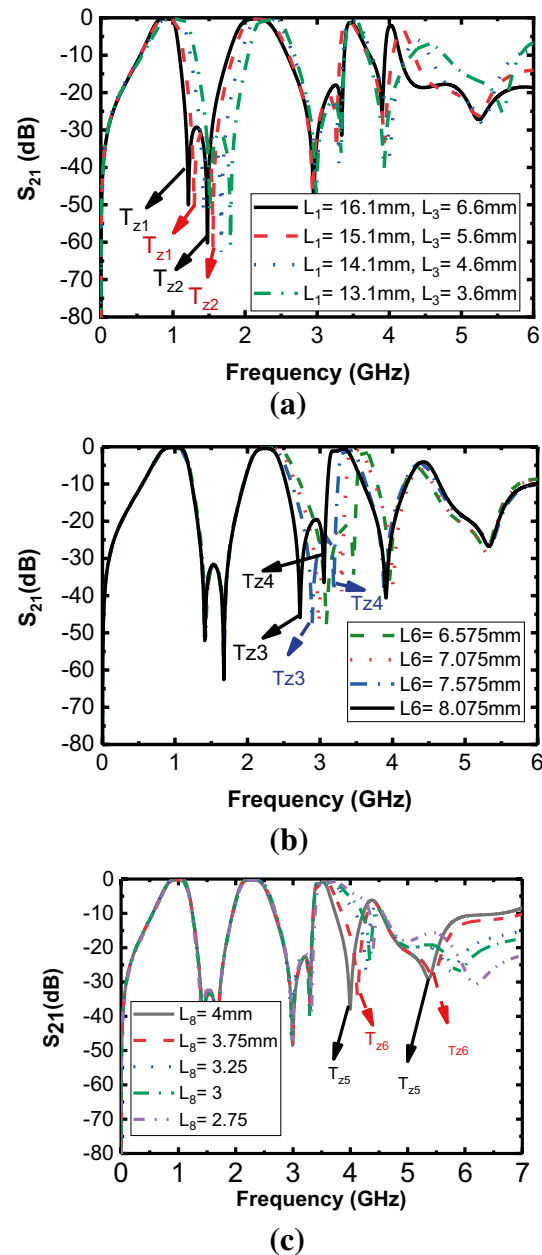


Fig. 3  $S_{21}$  versus frequency response of the tri-BPF in case of varying: a  $L_1$  and  $L_3$  b  $L_6$  c  $L_8$

zeros in the stop-band come closer to each other. So the intra stubs spacing is a crucial parameter which can also tune the respective bands of the BPF.

Similarly,  $L_5$  is the dimension of the short ended stub which is located in the middle of the resonator. Under the odd mode analysis, the length of the  $L_5$  stub is ignored while in even mode analysis  $L_5$  is counted to predict the resonant frequencies of even modes. So  $L_5$  only controls the even modes of all the bands in the given design. Therefore, this parameter can be used to tune the frequency of even mode which allows us to control the

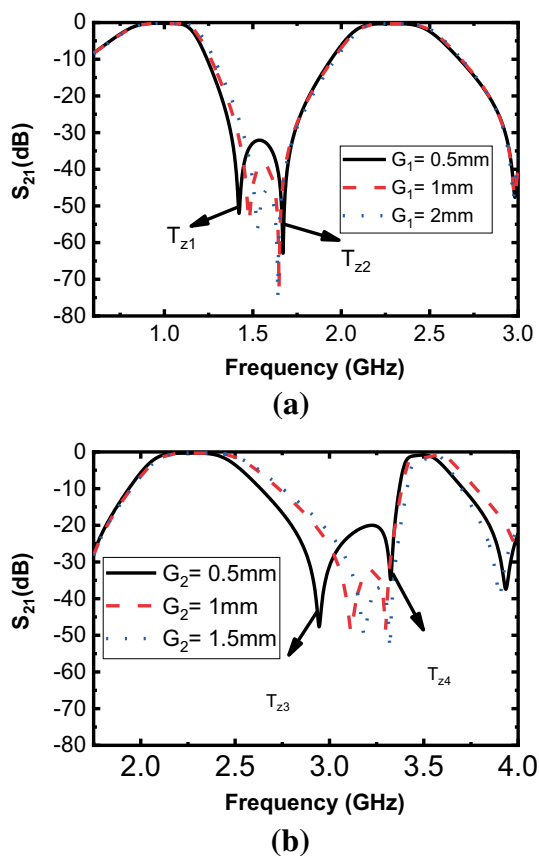


Fig. 4  $S_{21}$  versus frequency response in case of varying: **a**  $G_1$ , **b**  $G_2$

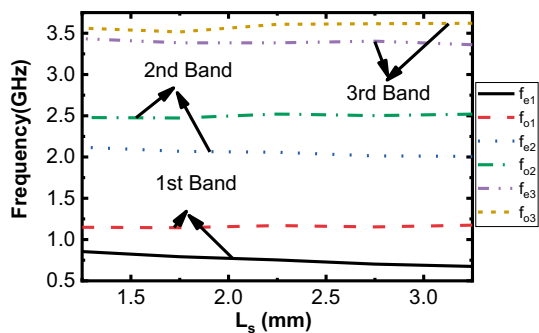


Fig. 5 Simulated resonant modes for various values of  $L_s$

**Table 1** Dimensions of the proposed Tri-band BPF (All values are given in mm)

Parameter	Value	Parameter	Value	Parameter	Value	Parameter	Value
$L_m$	5	$L_s$	2.25	$W_r$	2	$W_2$	1.75
$L_f$	3.25	$W_5$	1	$W_1$	0.5	$W_3$	2.175
$W_6$	1	$W_7$	4	$L_1$	14.1	$L_2$	4
$L_4$	4	$L_5$	7.025	$L_6$	7.07	$L_7$	5.85
$G_1, G_2, G_3$	0.5	Via	0.5	$W_4$	0.5	$W_5$	2.075
$L_3$	4.6	$L_8$	4				

bandwidths of all the passing bands using the length of the  $L_s$ . It is revealed in Fig. 5 that increasing the length of the  $L_s$  will tune down even mode frequencies which increases the overall bandwidth of all the passing bands.

### 4 Optimized design and fabrication of the proposed tri-BPF

In the previous section, the relation between the physical parameters of BPF and modal frequencies and bandwidths of passing bands are explained in detail. Based on the above parametric analysis, an optimized tri-band BPF design is presented and then fabricated for validation. All simulations are performed in Ansoft HFSS. The optimized geometrical parameters of the developed tri-band BPF are tabulated in Table 1. The circuit area of tri-band BPF is  $16.1 \text{ mm} \times 23.5 \text{ mm}$  ( $0.08\lambda_g \times 0.12\lambda_g$ ) excluding  $50 \Omega$  transmission line where  $\lambda_g$  signifies the guided wavelength of the middle frequency of the lowest passband. The layout shown in Fig. 2 is fabricated on Rogers RO4350 substrate having relative dielectric constant  $\epsilon_r = 3.66$  and loss tangent equal to 0.004. The thickness of the aforementioned substrate is 0.762 mm. The fabricated tri-band BPF is displayed in Fig. 6, as well.

The measured and simulated frequency response including  $S_{11}$  and  $S_{21}$  of the proposed tri-band BPF is also shown in Fig. 7. The proposed tri-band BPF is aimed for useful wireless applications such as GSM-900, LTE-2300, and WiMAX (3.5 GHz). The middle frequencies of the developed tri-band BPF are 0.9550 GHz, 2.2948 GHz, and 3.5246 GHz. The corresponding 3-dB fractional bandwidth of the stated center frequencies are 45.25%, 20.32% and 6.09% for the 1st, 2nd, and 3rd passbands, respectively. The measured insertion loss in the three pass-bands is 0.32, 0.63 and 1.38 including losses from the SMA connectors. Six transmission zeros are created in the simulated frequency response at frequencies 1.43 GHz, 1.68 GHz, 3.008 GHz, 3.33 GHz, 4.0 GHz and 5.33 GHz with more than 28 dB attenuations in order to get sharp skirt selectivity for the passbands. The presented tri-band BPF is compared with other recently reported designs and it is shown in Table 2.



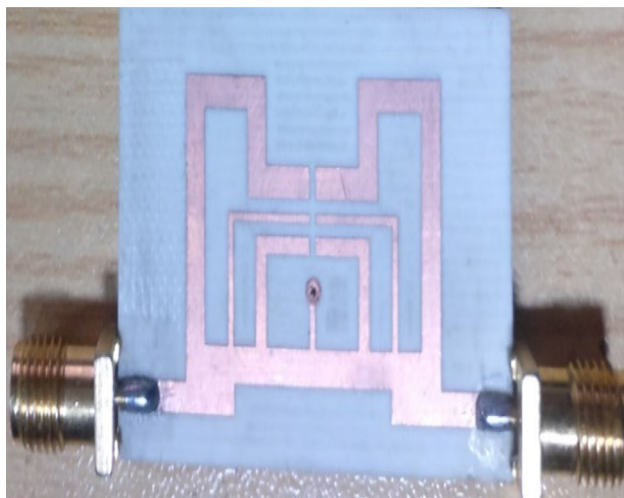


Fig. 6 Prototype of Tri-band BPF

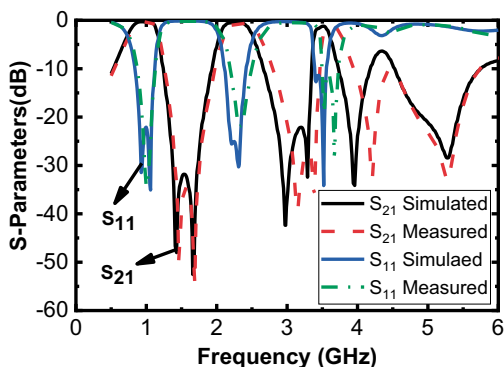


Fig. 7 Simulated and measured S-parameters of tri-band BPF

### 5 Quad-band BPF design and fabrication

Next we developed and fabricated a very compact quad band BPF as shown in Fig. 8. A quad-band BPF is developed using the same approach as used for tri

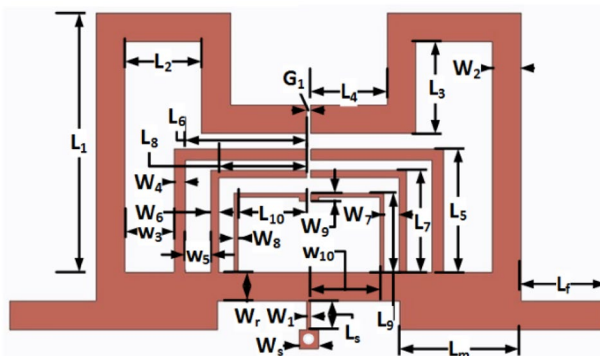


Fig. 8 Proposed quad-band BPF configuration

band BPF. Quad-band BPF response is achieved by incorporating two more identical open-ended stubs in the existing tri-band BPF described above. The meandered shape resonator is fed with 50-Ω transmission lines. The length and width parameters of the quad-band BPF are optimized using parametric analysis. The optimized parameters of the quad-band BPF design are listed in Table 3. The overall circuit area of the quad-band BPF is 17.1 mm × 23.5 mm (0.0912λ<sub>g</sub> × 0.125λ<sub>g</sub>). The proposed quad-band BPF is fabricated on the same Rogers RO4350 PCB having same thickness and dielectric constant i.e. 0.762 mm and 3.66 respectively. The fabricated prototype of quad-band BPF is also shown in Fig. 9.

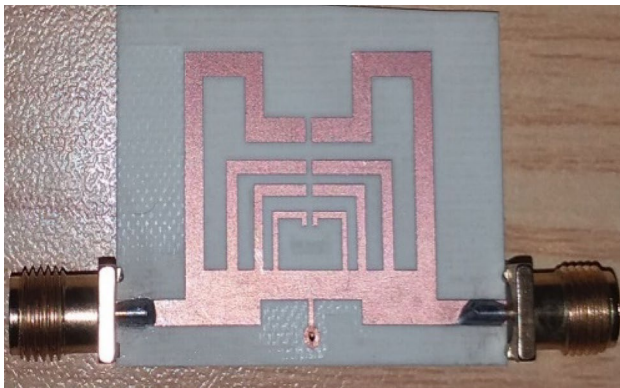
The frequency response of the measured and simulated results of quad-band BPF are given in Fig. 10. It is obvious that the measured and simulated frequency response agrees very well. The developed quad-band BPF is tuned for useful wireless applications which are GSM-900, LTE-2300, WiMAX (3.50 GHz) and WLAN (5.40 GHz). The operating frequencies of the quad-band BPF are 0.946 GHz, 2.2079 GHz, 3.59 GHz, and 5.4663 GHz. The percentage 3-dB fractional bandwidth all passbands are 42.64%, 21.31%, 7.074% and 7.414%,

Table 2 Performance comparison of proposed Tri-band BPF with other Tri-band BPF reported

Refs.	Center freq. (GHz)	3 dB Fractional band-width %	Circuit size in mm (λ <sub>g</sub> × λ <sub>g</sub> )	Tx zeros	S <sub>21</sub> (dB)
[2]	2.45/3.5/5.25	12.3/6.2/3.3	22.5 × 20.5 (0.24 × 0.22)	0	0.9/1.7/2.1
[3]	1.37/2.43/3.53	4.4/5.9/2.7	39.9 × 20.4 (0.26 × 0.13)	4	1.7/1.8/2.5
[12]	1.575/2.4/3.45	15.04/7.5/5.56	25.8 × 21 (0.18 × 0.14)	5	0.7/1.14/0.3
[13]	0.92/2.08/3.59	40.21/10.1/16.15	24 × 20 (0.13 × 0.10)	6	0.41/1.39/1.97
[20]	1.25/3.51/6.82	24.4/18.3/13.8	27.4 × 26.05 (0.156 × 0.149)	5	0.45/0.42/1.26
[21]	2.65/4.85/7.59	5.3/8.66/3.95	26 × 1.2 (0.60 × 0.02)	5	1.2/1.4
Tri-band BPF in this work	0.955/2.2948/3.524	45.25/20.32/6.09	16.1 × 23.5 (0.08 × 0.12)	6	0.32/0.63/1.38

**Table 3** Dimension of the Quad-band BPF (All values are given in mm)

Parameter	Value	Parameter	Value	Parameter	Value	Parameter	Value
$L_m$	7	$L_5$	2	$W_r$	2	$W_2$	1.75
$L_f$	3.25	$W_5$	1	$W_1$	0.5	$W_3$	2.175
$W_6$	0.8	$W_7$	0.95	$L_1$	15.1	$L_2$	4
$L_4$	4	$L_5$	7.5	$L_6$	6.575	$L_7$	5.85
$W_8$	0.5	$W_9$	1	$W_{10}$	2.75	$L_9$	4
$G_1, G_2, G_3, G_4$	0.5	Via	0.5	$W_4$	1	$W_5$	1.575
$L_3$	4.6	$L_8$	4.2	$L_{10}$	2.75		



**Fig. 9** Prototype of quad-band BPF

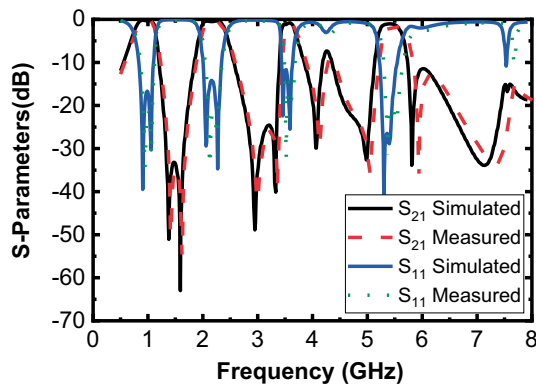


**Fig. 10** Simulated versus measured response of quad-band BPF

respectively. The measured insertion loss of all the four passbands at their center frequencies including SMA connectors are 0.31 dB, 0.56 dB, 1.59 dB, and 1.63 dB respectively. Seven transmission zeros are generated with more than 28 dB attenuation at 1.39 GHz, 1.60 GHz, 2.98 GHz, 3.36 GHz, 4.11 GHz, 5.05 GHz, and 5.88 GHz in order to get high selectivity pass-band filter response. Quad-band BPF is compared with other published works in the literature in Table 4. It is clear from the comparison table that the proposed quad-band BPF is advantageous in terms of insertion loss, circuit size, 3-dB fractional bandwidth, and maximum passbands along with maximum transmission zeros.

### 6 External quality factor and coupling coefficient

The analysis of the coupling coefficient and external quality factor of the filter was carried out and showed that the parameter 'G1' was able to control electric coupling. The magnetic coupling is actually a function of the distance between the two resonators. This magnetic coupling is very difficult to exactly calculate in such a complicated structure, so it is optimized using EM simulation. However, we have calculated the electric coupling coefficient "K<sub>e</sub>" versus "G<sub>1</sub>" using Eq. (11):

$$k_e = \frac{f_h^2 - f_l^2}{f_h^2 + f_l^2} \tag{11}$$

**Table 4** Performance comparison of the proposed quad BPF with recently published ones in the literature

Refs.	Center freq. (GHz)	3-dB Fractional bandwidth %	Circuit size in mm ( $\lambda_g \times \lambda_g$ )	Tx zeros	$S_{21}$ (dB)
[18]	2.40/3.5/5.20/6.8	6.4/9.4/3.8/4.9	22×20 (0.24×0.22)	2	0.5/1.3/1.3/1.0
[19]	1.5/2.50/3.50/5.2	5.7/14.1/6.9/3.8	26×26 (0.18×0.18)	5	1.3/0.24/1.29/2.1
[20]	1.19/3.33/5.87/8.39	20/13.6/7.6/15.4	25.8×21 (0.169×0.12)	7	0.6/0.52/1.58/1.3
[22]	1.46/2.6/4.2/5.25	8.6/4.5/5.2/4.2	17.2×15 (0.14×0.12)	4	1.5/1.9/1.7/2
Quad-band BPF in this work	0.94/2.20/3.59/5.46	42.64/21.31/7.07/7.41	17.1×23.5 (0.0912×0.12)	7	0.31/0.57/1.59/1.63

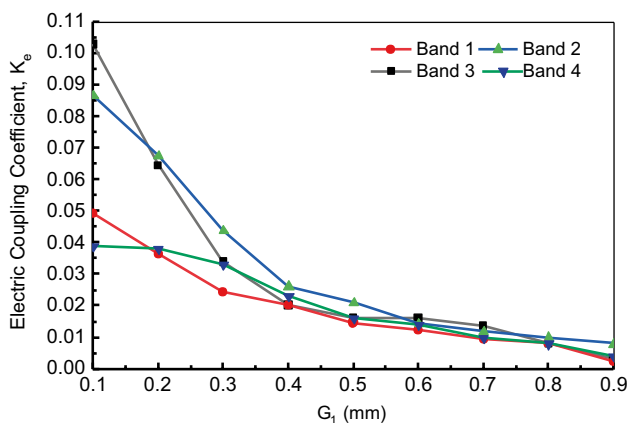


**Fig. 11** Electric coupling coefficient ' $K_e$ ' versus parameter ' $G_1$ ' of the proposed quad band bandpass filter. ( $G_1 = G_2 = G_3 = G_4$ )

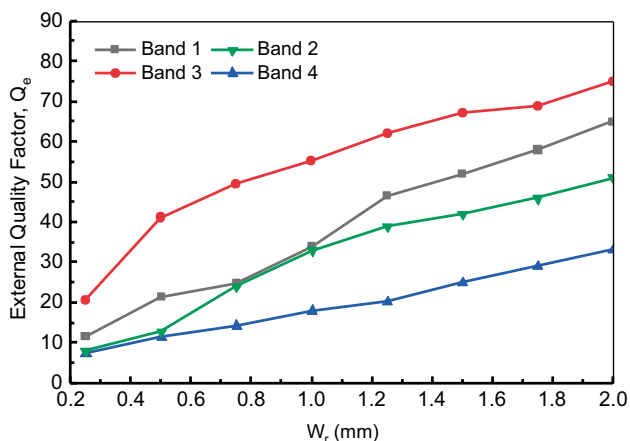


**Fig. 12** External quality factor ' $Q_e$ ' versus parameter ' $W_r$ ' of the proposed quad band bandpass filter

where  $f_l$  and  $f_h$  represent the lower and higher frequencies of the two resonant frequency bands. Also, the external quality factor, " $Q_e$ " can be calculated from full wave simulated transmitted coefficients given by [17] as:

$$Q_e = \frac{\omega_0}{\Delta\omega_{(3\text{dB})}} \tag{12}$$

The electric coupling coefficient of the proposed filter is dependent on parameter ' $G_1$ ' and is plotted in Fig. 11. It is seen that as the distance ' $G_1$ ' increases, the corresponding electric coupling also decreases as expected. It must be noted that  $G_1 = G_2 = G_3 = G_4$ , which is the corresponding distances between the first, second, third, and fourth resonators. For convenience it has been represented as  $G_1$  only in Fig. 11. However, it is observed that the distance ' $G_1$ ' have a different influence on different passbands. The external quality factor of the proposed bandpass filter

is also calculated from Eq. (12) and it is plotted with the parameter ' $w_r$ ' in Fig. 12.

### 7 Conclusion

A compact tri and quad band BPFs using SLR are presented for wireless applications. The proposed resonator is analyzed by means of even-odd mode analysis due to its symmetrical geometry. Open-ended stubs are loaded at an appropriate position in the dual-mode resonator and we have successfully achieved tri and quad passbands. To reduce the filter size and create transmission zeros at the desired frequencies in the stop-bands, a symmetrical meandered shape resonator is loaded with open-ended identical stubs which are bent towards each other. The proposed BPFs are tune to operate at GSM-900, LTE-2300, WiMAX (3.50 GHz), and WLAN (5.40 GHz) bands. Significant improvements are observed in terms of circuit size, 3-dB fractional bandwidth, insertion loss and transmission zeros. To check the validity of the proposed tri and quad BPFs, these designs are simulated in HFSS, fabricated and then measured using network analyzer. The measured and simulated responses in both cases agree very well. The proposed BPFs can find applications in multiband wireless communication systems.

### Compliance with ethical standards

**Conflict of interest** The authors declare that they have no competing interests.

### References

- Zhang XY, Chen JX, Xue Q, Li SM (2007) Dual-band bandpass filters using stub-loaded resonators. *IEEE Microw Wirel Compon Lett* 17:583–585
- Liang LC, Di H, Wu B (2010) Design of tri-band filter based on stub loaded resonator and DGS resonator. *IEEE Microw Wirel Compon Lett* 20:265–267
- Lan SW, Weng MH, Chang SJ, Hung CY, Liu SK (2015) A tri-band bandpass filter with wide stopband using asymmetric stub loaded resonators. *IEEE Microw Wirel Compon Lett* 25(1):19–21
- Rahman M, Khan WT, Imran M (2018) Penta-notched UWB antenna with sharp frequency edge selectivity using combination of SRR, CSRR, and DGS. *Int J Electron Commun (AEÜ)* 93:116–122
- Sami A, Rahman M (2019) A very compact quintuple band bandpass filter using multimode stub loaded resonator. *Prog Electromagn Res* 93:211–222
- Rahman M, NagshvarianJahromi M, Mirjavadi SS, Hamouda AM (2019) Compact UWB band-notched antenna with integrated bluetooth for personal wireless communication and UWB applications. *Electronics* 8:158



7. Ghazali AN, Sazid M, Pal S (2017) A compact broadside coupled dual notched band UWB-BPF with extended stopband. *Int J Electron Commun (AEÜ)* 82:502–507
8. Lai X, Liang C-H, Di H, Wu B (2010) Design of tri-band filter based on stub loaded resonator and DGS resonator. *IEEE Microw Wirel Compon Lett* 20(5):265–267
9. Luo S, Zhu L, Sun S (2011) Compact dual-mode triple-band bandpass filters using three pairs of degenerate modes in a ring resonator. *IEEE Trans Microw Theory Tech* 59(5):1222–1229
10. Kumar N, Singh Y (2014) Compact tri-band bandpass filter using three stub-loaded open loop resonator with wide stopband and improved bandwidth response. *Electron Lett* 50(25):1950–1952
11. Cho Y-H, Yun S-W (2014) A tri-band bandpass filter using stub loaded SIRS with controllable bandwidths. *Microw Opt Technol Lett* 56(12):2907–2910
12. Rahman M, Park J-D (2018) A compact tri-band bandpass filter using two stub-loaded dual mode resonators. *Prog Electromagn Res* 64:201–209
13. Murmu L, Das SD, Bage A (2016) A compact tri-band bandpass filter using multi-mode stub loaded resonator. In: *Proceedings of the Asia-Pacific microwave conference 2016*
14. Rahman M, Naghshvarian Jahromi M, Mirjavadi S, Hamouda A (2018) Bandwidth enhancement and frequency scanning array antenna using novel UWB filter integration technique for OFDM UWB radar applications in wireless vital signs monitoring. *Sensors* 18(9):3155
15. Rahman M, Ko DS, Park JD (2018) A compact tri-band bandpass filter utilizing double mode resonator with 6 transmission zeros. *Microw Opt Technol Lett* 60(7):1767–1771
16. Jahromi MN (2011) Wide stopband compact microstrip lowpass filter using circular ring resonator and split ring resonators. *Microw Opt Technol Lett* 53(9):1961–1964
17. Hejazi ZM (2012) A fast design approach of compact microstrip multiband bandpass filters. *Microw Opt Technol Lett* 54(4):1075–1079
18. Wu HW, Yang RY (2011) A new quad-band bandpass filter using asymmetric stepped impedance resonator. *Microw Wirel Compon Lett* 21(4):203–205
19. Huang WFQ, Shi X-W (2014) A compact quadband bandpass filter using novel stub loaded SIR structure. *Microw Opt Technol Lett* 56(3):538–542
20. Wu XJW, Miao C (2013) Compact microstrip dual-/tri-/quad-band bandpass filter using open stubs loaded shorted stepped-impedance resonator. *IEEE Trans Microw Theory Tech* 61(9):3187–3199
21. Xiao J-K, Zhu Y-F (2014) Multi-band bandstop filter using inner T-shaped defected microstrip structure (DMS). *Int J Electron Commun (AEÜ)* 68(2):90–96
22. Gao L, Zhang XY, Zhao X-L, Zhang Y, Xu J-X (2016) Novel compact quad-band bandpass filter with controllable frequencies and bandwidths. *IEEE Microw Wirel Compon Lett* 26(6):395–397

**Publisher's Note** Springer Nature remains neutral with regard to jurisdictional claims in published maps and institutional affiliations.